data

MDPI

Data Descriptor

Datasets for the Determination of Evaporative Flux from Distilled Water and Saturated Brine Using Bench-Scale Atmospheric Simulators

Jared Suchan and Shahid Azam *

Faculty of Engineering and Applied Science, University of Regina, 3737 Wascana Parkway, Regina, SK S4S 0A2, Canada; suchan1j@uregina.ca
* Correspondence: shahid.azam@uregina.ca

Abstract: Evaporation from fresh water and saline water is critical for the estimation of water budget in the Canadian Prairies. Predictive models using empirical field-based data are subject to significant errors and uncertainty. Therefore, highly controlled test conditions and accurately measured experimental data are required to understand the relationship between atmospheric variables at water surfaces. This paper provides a comprehensive dataset generated for the determination of evaporative flux from distilled water and saturated brine using the bench-scale atmospheric simulator (BAS) and the subsequently improved design (BAS2). Analyses of the weather scenarios from atmospheric parameters and evaporative flux from the experimental data are provided.

Dataset: doi:10.5683/SP3/JJ2FS6.

Keywords: evaporative flux; distilled water; saturated brine; bench-scale atmospheric simulator

Citation: Suchan, J.; Azam, S. Datasets for the Determination of Evaporative Flux from Distilled Water and Saturated Brine Using Bench-Scale Atmospheric Simulators. *Data* **2022**, *7*, 1. https://doi.org/10.3390/data7010001

Academic Editor: Vladimir Sreckovic

Received: 10 November 2021
Accepted: 15 December 2021
Published: 22 December 2021

1. Summary

The Canadian Prairies experience the highest annual water yield variability in the country owing to an inland physiographic climate and a glacial geomorphology [1]. The regional climate is characterized by windy, dry, warm, and sunny conditions [2]. Likewise, the terrain is generally flat, containing interconnected shallow lakes originating from melting waters during the glacial retreat [3]. These unique features result in high evaporation rates from waterbodies, thereby reducing the volume of surface water for municipal, agricultural, and industrial uses [4]. For example, the surface area of Lake Diefenbaker (largest man-made reservoir in the region) varies from 102–430 km^2, with an estimated water loss of 1–4.3 $\times$ 10^6 m^3 for an elevation drop of 10 mm [5]. Furthermore, the region has numerous salt-rich lakes and potash tailings ponds [6]. Evaporation from these hypersaline facilities is critical for the protection of wildlife habitats and for recycling of processed water, respectively [7].

Evaporation prediction models developed using empirical field-based data are subject to significant errors and uncertainty owing to natural atmospheric variations and absence of direct evaporative flux measurements [8]. To understand the relationship between atmospheric variables at water surfaces, highly controlled test conditions and accurately measured experimental data are required. Several laboratory-based evaporation experiments using climate simulators have been developed [9]. The main limitations of these methods are the limited number of controlled parameters and the quality of their simulation [10]. The authors developed a state-of-the-art bench-scale atmospheric simulator (BAS) to determine evaporative fluxes. Initially used for water surfaces [11], the instrument was improved and named BAS2 [10] and was subsequently used for water and brine surfaces [12]. The instrument can simultaneously control and/or measure air velocity,

humidity, air temperature, incoming shortwave solar irradiance, outgoing shortwave surface reflectance, surface temperature, and barometric pressure. The generated datasets are critical for developing a comprehensive understanding of the effects of atmospheric parameters on the rate of evaporation under laboratory conditions. Based on the climatic conditions of the Canadian prairies, the datasets provide a baseline for correlating with monitoring data under actual field conditions and for calibrating predictive models under various hypothetical scenarios.

The main purpose of this paper is to provide a comprehensive dataset generated for the determination of evaporative flux from distilled water and saturated brine using BAS and BAS2 configurations [13]. Analyses of the weather scenarios from atmospheric parameters and evaporative flux from the experimental data are provided. The manuscript is divided into two main sections. The data description section provides context to the origin of the datasets, an outline of the folder structure containing the various datasets, and a description of the contents and variables in each dataset. Likewise, the methodology section provides a description of the weather scenario development, sample preparation and equipment operations, and Equations required to calculate the relevant parameters for evaporation estimation.

2. Data Description

Figure 1 presents the file structure of the folders containing test data. The "Liquid Evaporation" root folder contains two main subfolders, namely "1. Prairie Climate" and "2. Evaporation Experiments". The datasets in these folders are organized and described in the following tables.

Table 1 presents a description of the dataset variables in the Prairie Climate folder. The "1. Prairie Climate" folder contains the data used to construct six weather scenarios. Atmospheric data are contained in the folder "1. Atmosphere", where five separate data files provide 16 years of hourly measurements of air velocity, humidity, air temperature, and solar irradiance from the Canadian Weather Energy and Engineering Datasets (CWEEDS). Four separate datasets for Kindersley, Regina, Swift Current, and Wynyard were developed. These contain processed variables and are linked to the fifth workbook, "Gardiner", where variables are determined for a select point on Lake Diefenbaker using an inverse-distance weighting equation as described by Suchan and Azam [11]. Surface data for all of the above locations are contained in the folder "2. Surface", where a data file provides mean values of 17 years of 8-day daytime and nighttime surface temperature values collected by [14].

Table 2 presents a description of the dataset variables in the "2. Evaporation Experiments" folder obtained using BAS [11] and BAS2 [10]. The "1. BAS" contains data for distilled water evaporation experiments using all six weather scenarios. In the "2. BAS2" folder, the "1. Null" folder contains datasets for all six daytime weather scenarios without a liquid sample for the purpose of calibration of the setup. Furthermore, this folder contains separate sub-folders for distilled water ("2. Water") and saturated brine ("3. Brine") using all six weather scenarios. Each test scenario for each liquid includes "1. Raw Data" and "2. Data Summary" sub-folders. The "1. Raw Data" contain eight data files that were generated during testing, namely air pressure, air temperature and humidity (four datasets from four different sensor locations), air velocity, surface temperature, and sample weight. These folders contain one data file that combines all the raw data in a single dataset.

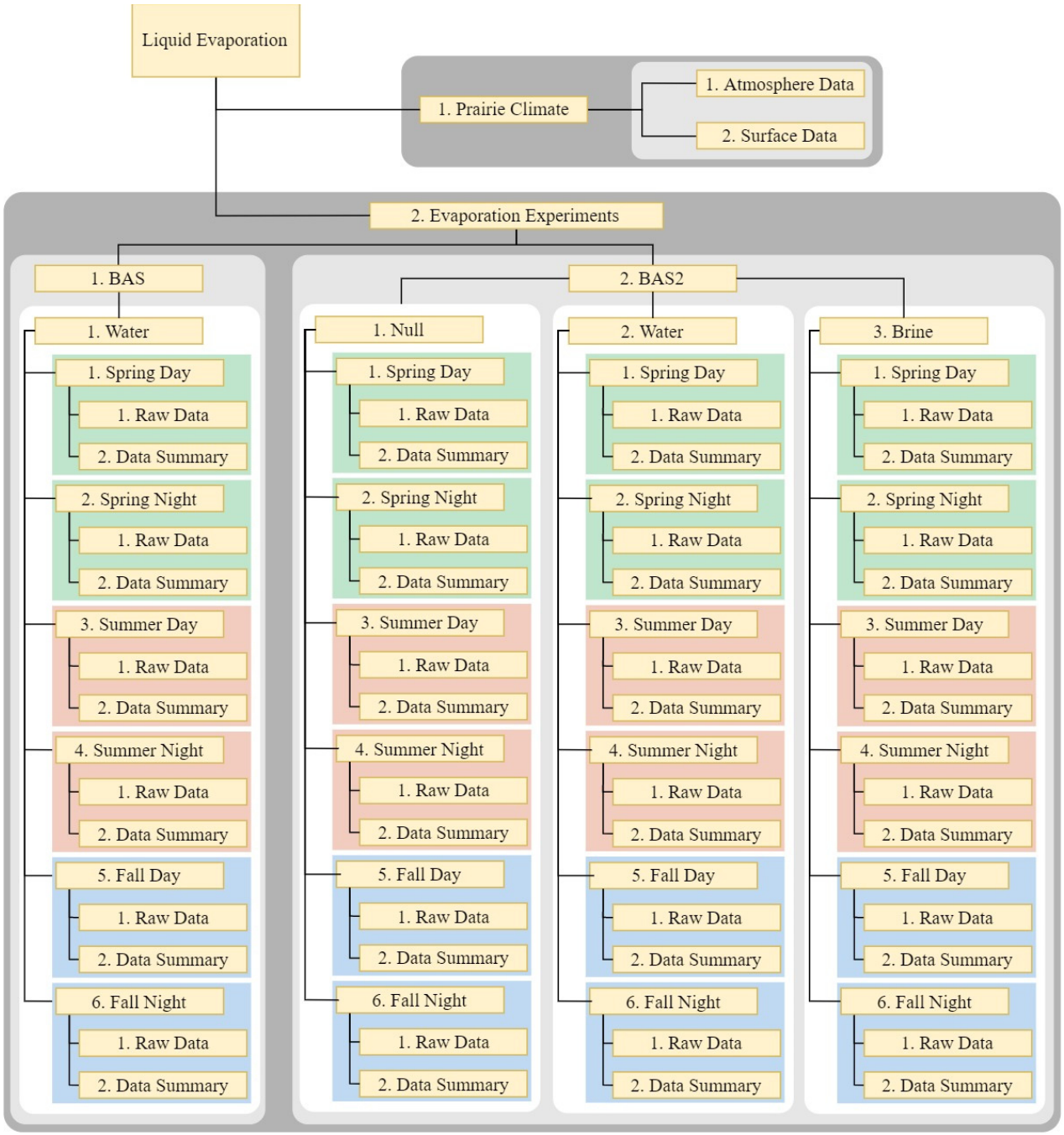

Figure 1. File structure of the folders containing data.

Table 1. Description of the dataset variables in the Prairie Climate folder.

Variable	Units	Description
Atmosphere Data Folder, Local Climate Datasets		
Data Info Tab		*Contains details on the weather station.*
Hourly Data Tab		*Contains hourly CWEEDS weather station measurements and data conversions.*
Year		Date format in YYYY.
Month		Date format in MM.
Day		Date format in DD.

Table 1. *Cont.*

Variable	Units	Description
Hour		Date format in HH.
Global Horizontal Irradiance	kJ/h	The rate of radiative solar energy delivered to the surface.
Global Horizontal Irradiance Converted	W/m^2	The radiative solar energy flux imposed on the surface.
Dry Bulb Temperature	°C	The temperature of the air measured by a thermometer shieled from solar radiation and moisture.
Dew Point Temperature	°C	The temperature required for partial vapor pressure to equal saturated vapor pressure, assuming constant air pressure and atmospheric water content.
Absolute Humidity	g/m^3	The atmospheric water content.
Relative Humidity	%	The ratio of partial vapor pressure to saturated vapor pressure.
Wind Speed	m/s	The velocity of the air measured at 10 m above the surface.
Wind Speed Converted	m/s	The velocity of the air measured at 0.03 m above the surface.
Daily Data Tab		*Hourly measurements averaged into daily values throughout the dataset and subdivided into daytime and nighttime components.*
Year		Date format in YYYY.
Month		Date format in MM.
Day		Date format in DD.
All Temperature	°C	Mean daily (24 h) temperature.
Day Temperature	°C	Mean air temperature during the day, using hourly measurements in the 24 h period where extraterrestrial radiation was greater than zero.
Night Temperature	°C	Mean air temperature at night, using hourly measurements in the 24 h period where extraterrestrial radiation was equal to zero.
All Humidity	g/m^3	Mean daily (24 h) absolute humidity.
Day Humidity	g/m^3	Mean absolute humidity during the day, using hourly measurements in the 24 h period where extraterrestrial radiation was greater than zero.
Night Humidity	g/m^3	Mean absolute humidity at night, using hourly measurements in the 24 h period where extraterrestrial radiation was equal to zero.
All Relative Humidity	%	Mean daily (24 h) relative humidity.
Day Relative Humidity	%	Mean relative humidity during the day, using hourly measurements in the 24 h period where extraterrestrial radiation was greater than zero.
Night Relative Humidity	%	Mean relative humidity at night, using hourly measurements in the 24 h period where extraterrestrial radiation was equal to zero.
All Wind	m/s	Mean daily (24 h) wind speed.
Day Wind	m/s	Mean wind speed during the day, using hourly measurements in the 24 h period where extraterrestrial radiation was greater than zero.
Night Wind	m/s	Mean wind speed at night, using hourly measurements in the 24 h period where extraterrestrial radiation was equal to zero.
All Irradiance	W/m^2	Mean daily (24 h) solar irradiance.
Extraterrestrial Irradiance	W/m^2	Mean solar irradiance on the surface during the day, using hourly measurements in the 24 h period where extraterrestrial radiation was greater than zero.
Night Irradiance	W/m^2	Mean solar irradiance on the surface during the day at night, using hourly measurements in the 24 h period where extraterrestrial radiation was equal to zero.
Daily Mean Tab		*Daily values averaged into daily means for each day throughout the year, including daytime and nighttime components.*
No.		Day number of the year, out of 365.
Month		Date format in MM.
Day		Date format in DD.
Temperature—Mean	°C	Mean air temperature for the given day of the year.
Day Temperature—Day	°C	Mean air temperature during the daytime for the given day of the year.
Temperature—Night	°C	Mean air temperature during the nighttime for the given day of the year.

Table 1. *Cont.*

Variable	Units	Description
Humidity—Mean	g/m^3	Mean absolute humidity for the given day of the year.
Humidity—Day	g/m^3	Mean absolute humidity during the daytime for the given day of the year.
Humidity—Night	g/m^3	Mean absolute humidity during the nighttime for the given day of the year.
Wind Speed—Mean	m/s	Mean air velocity for the given day of the year.
Wind Speed—Day	m/s	Mean air velocity during the daytime for the given day of the year.
Wind Speed—Night	m/s	Mean air velocity during the nighttime for the given day of the year.
Irradiance—Mean	W/m^2	Mean solar irradiance for the given day of the year.
Irradiance—Day	W/m^2	Mean solar irradiance during the daytime for the given day of the year.
Irradiance—Night	W/m^2	Mean solar irradiance during the nighttime for the given day of the year.
Relative Humidity—Mean	g/m^3	Mean relative humidity for the given day of the year.
Relative Humidity—Day	g/m^3	Mean relative humidity during the daytime for the given day of the year.
Relative Humidity—Night	g/m^3	Mean relative humidity during the nighttime for the given day of the year.
Monthly Mean Tab		*Hourly measurements averaged into monthly means for each month of the year, and subdivided into daytime and nighttime components.*
Count		Monthly Mean day number of the year, out of 365.
Month		Month number of the year, out of 12.
Temperature—Mean	°C	Mean air temperature for the given month of the year.
Temperature—Mean SD	°C	Standard deviation of air temperature for the given month of the year.
Temperature—Daytime Monthly Mean	°C	Mean air temperature during the daytime for the given month of the year.
Temperature—Day SD	°C	Standard deviation air temperature during the daytime for the given month of the year.
Temperature—Nighttime Monthly Mean	°C	Mean air temperature during the nighttime for the given month of the year.
Temperature—Night SD	°C	Standard deviation air temperature during the nighttime for the given month of the year.
Humidity—Mean	g/m^3	Mean absolute humidity for the given month of the year.
Humidity—Mean SD	g/m^3	Standard deviation of absolute humidity for the given month of the year.
Humidity—Daytime Monthly Mean	g/m^3	Mean absolute humidity during the daytime for the given month of the year.
Humidity—Day SD	g/m^3	Standard deviation absolute humidity during the daytime for the given month of the year.
Humidity—Nighttime Monthly Mean	g/m^3	Mean absolute humidity during the nighttime for the given month of the year.
Humidity—Night SD	g/m^3	Standard deviation absolute humidity during the nighttime for the given month of the year.
Wind Speed—Mean	m/s	Mean air velocity for the given month of the year.
Wind Speed—Mean SD	m/s	Standard deviation of air velocity for the given month of the year.
Wind Speed—Daytime Monthly Mean	m/s	Mean air velocity during the daytime for the given month of the year.
Wind Speed—Day SD	m/s	Standard deviation air velocity during the daytime for the given month of the year.
Wind Speed—Nighttime Monthly Mean	m/s	Mean air velocity during the nighttime for the given month of the year.
Wind Speed—Night SD	m/s	Standard deviation air velocity during the nighttime for the given month of the year.
Irradiance—Mean	W/m^2	Mean solar irradiance for the given month of the year.
Irradiance—Mean SD	W/m^2	Standard deviation of solar irradiance for the given month of the year.

Table 1. *Cont.*

Variable	Units	Description
Irradiance—Daytime Monthly Mean	W/m^2	Mean solar irradiance during the daytime for the given month of the year.
Irradiance—Day SD	W/m^2	Standard deviation solar irradiance during the daytime for the given month of the year.
Irradiance—Nighttime Monthly Mean	W/m^2	Mean solar irradiance during the nighttime for the given month of the year.
Irradiance—Night SD	W/m^2	Standard deviation solar irradiance during the nighttime for the given month of the year.
Relative Humidity—Mean	%	Mean relative humidity for the given month of the year.
Relative Humidity—Mean SD	%	Standard deviation of relative humidity for the given month of the year.
Relative Humidity—Daytime Monthly Mean	%	Mean relative humidity during the daytime for the given month of the year.
Relative Humidity—Day SD	%	Standard deviation relative humidity during the daytime for the given month of the year.
Relative Humidity—Nighttime Monthly Mean	%	Mean relative humidity during the nighttime for the given month of the year.
Relative Humidity—Night SD	%	Standard deviation relative humidity during the nighttime for the given month of the year.
Surface Data Folder, Lake Diefenbaker Water Surface Temperature Dataset		
Day		Date format in DD.
Month		Date format in MM.
Day Temperature	°C	Mean surface temperature during the daytime for the given day and month of the year.
Night Temperature	°C	Mean surface temperature during the nighttime for the given day and month of the year.

Table 2. Description of the dataset variables in the evaporation experiments folder.

Variable	Units	Description
Raw Data Folder, Air Pressure Datasets		
Index		Measurement counter.
Date		Date format in DD/MM/YYYY
Time		Time format in HH:MM:SS
°C	°C	Measured air temperature at the barometer location.
%RH	%	Measured relative humidity at the barometer location.
hPa	hPa	Measured air pressure at the barometer location.
Pa	Pa	Converted air pressure value.
Raw Data Folder, Air Temperature-Air Humidity		
No.		Measurement counter.
Time		Time and date format in YYYY-MM-DD HH:MM:SS
Temperature°C	°C	Measured air temperature at the indicated thermometer location.
Humidity%	%	Measured relative humidity at the indicated hygrometer location.
Raw Data Folder, Air Velocity		
Index		Measurement counter.
Time		Time format in HH:MM:SS
Wind Value(m/s)	m/s	Measured air velocity at the anemometer location.
Temp(°C)	°C	Measured air temperature at the anemometer location.
Raw Data Folder, Surface Temperature		
DataPoint		Measurement counter.

Table 2. *Cont.*

Variable	Units	Description
LogDate		Date format in YYYY-MM-DD.
LogTime		Time format in HH:MM:SS AM/PM.
°C	°C	Measured sample surface temperature.
Raw Data Folder, Sample Weight		
Column A		Date format in DD.MM.YYYY.
Column B		Time format in HH:MM:SS.
Column C	g	Measured sample weight.
Data Summary Folder, Data Summary Datasets		
Time		Time format in HH:MM:SS AM/PM.
Count		Measurement counter.
Minutes		Time format in M.MM.
Hours		Time format in H.HHH.
Velocity	m/s	Measured air velocity at the anemometer location.
Aerodynamic Resistance	s/m	Calculated aerodynamic resistance using (Equation (30)).
Air Pressure	Pa	Measured air pressure at the barometer location.
Air Pressure Interpolated	Pa	Calculated air pressure at 10-s intervals using linear Equation between 30-s intervals.
Psychrometric Constant	Pa/°C	Calculated psychrometric constant using (Equation (31)).
Relative Humidity	%	Measured relative humidity at the indicated hygrometer location.
Air Density	g/m^3	Calculated air density using (Equation (1)).
Vapour Density	g/m^3	Calculated absolute humidity using (Equation (9)).
Partial Vapour Pressure	Pa	Calculated partial vapor pressure using (Equation (5)).
Air Saturated Vapour Pressure	Pa	Calculated atmospheric saturated vapor pressure using (Equation (7)) with T_a.
Deficit Vapour Pressure	Pa	Calculated atmospheric vapor pressure deficit using (Equation (8)).
Gradient Vapour Pressure	Pa	Calculated vapor pressure gradient using (Equation (32)).
Dew Point Temperature	°C	Calculated dew point temperature using (Equation (6)).
Mole Fraction Water Vapour		Calculated mole fraction of water vapor using (Equation (2)).
Enhancement Factor		Calculated enhancement factor of water vapor using (Equation (3)).
Compressibility Factor		Calculated compressibility factor of water vapor using (Equation (4)).
Incoming Shortwave Radiant Heat Flux	W/m^2	Calibrated incoming solar irradiance.
Air Temperature	°C	Measured air temperature at the indicated thermometer location.
Air Emissivity		Calculated longwave emissivity of the atmosphere above the sample using (Equation (21)).
Incoming Longwave Radiant Heat Flux	W/m^2	Calculated incoming infrared radiant energy using (Equation (20)).
Sample Mass Measured	g	Measured sample mass.
Sample Mass Interpolated	g	Calculated sample mass using a polynomial regression.
Sample Mass Rate of Change	g/s	Calculated change in sample mass using (Equation (11)).
Air Saturated Water Density	g/m^3	Calculated air saturated density of water using (Equation (15)).
Isothermal Compressibility		Calculated isothermal compressibility using (Equation (16)).
Corrected Water Density	g/m^3	Calculated corrected water density using (Equation (14)).
Sample Volume	m^3	Calculated sample volume using (Equation (13)).
Sample Surface Area	m^2	Calculated sample surface area using (Equation (12)).
Surface Saturated Vapour Pressure	Pa	Calculated atmospheric saturated vapor pressure using (Equation (7)) with T_s.
Total Vapour Flux	$g/s \cdot m^2$	Calculated evaporative flux using (Equation (10)).
Evaporation Rate	mm/day	Calculated rate of evaporation using (Equation (33)).
Outgoing Shortwave Radiant Heat Flux	W/m^2	Measured outgoing solar irradiance.
Corrected Outgoing Shortwave Radiant Heat Flux	W/m^2	Corrected outgoing solar irradiance using (Equation (21)).

Table 2. *Cont.*

Variable	Units	Description
Surface Temperature	°C	Measured sample surface temperature.
Outgoing Longwave Radiant Heat Flux	W/m^2	Calculated outgoing infrared radiant energy using (Equation (23)).
Net Radiant Heat Flux	W/m^2	Calculated net radiant heat flux at the surface using (Equation (19)).
Bowen Ratio		Calculated Bowen Ratio using (Equation (28)).
Sensible Thermal Heat Flux	W/m^2	Calculated atmospheric thermal heat flux using (Equation (27)).
Conductive Thermal Heat Flux	W/m^2	Calculated ground heat flux using (Equation (29)).
Available Energy	W/m^2	Calculated available energy using (Equation (18)).
Evaporative Latent Heat	J/g	Calculated evaporative latent heat energy using (Equation (26)).
Evaporative Latent Heat Flux	W/m^2	Calculated evaporative latent heat flux using (Equation (24)).
Evaporative Latent Heat Flow	W	Calculated evaporative latent heat flow using (Equation (25)).

3. Methods

Figure 2 presents a summary of surface-atmosphere conditions in the semi-arid Canadian Prairies, and Table 3 presents the six weather scenarios developed by Suchan and Azam [11] for the evaporation experiments. The surface-atmosphere conditions include the monthly averages and standard deviations of five controlled parameters, including (a) air velocity, (b) humidity, (c) air temperature, (d) solar irradiance, and (e) surface temperature. The six weather scenarios were formed by dividing annual conditions into diurnal components of daytime (Figure 2, left column) and nighttime (Figure 2, right column). In each case, the three seasons of spring, summer, and fall were demarcated for evaporation, whereas winter was excluded due to the prevalent freezing conditions. The parameters in each season were chosen by selecting a value near the monthly mean and extending horizontally, using monthly standard deviations as a guide for cut-off boundaries.

The detailed operation procedure to simulate these six weather scenarios in the BAS, in addition to the sample preparation methods for water-based experiments, are provided by Suchan and Azam [11]. The methods for the brine-based experiments are given in Suchan and Azam [12], while the operation procedure of the BAS2 is provided by Suchan and Azam [10].

For null experiments, BAS2 was operated for about 1.0 h without any sample to establish sensor baseline values. For water experiments, the sample container was cleaned, allowed to air dry, and placed on the analytical scale balance in the simulator. Approximately 15 mL of water was added to the container, and the evaporation tests were conducted for approximately 3.0 h and 1.5 h in BAS and BAS2, respectively. For brine experiments, the same protocol was followed using 15 mL of a hypersaline stock solution (36 g of NaCl in 100 mL of distilled water). To accommodate the slower evaporation rates, these experiments were conducted for approximately 6.0 h [12]. To operate BAS and BAS2, the required modules (solar irradiance, air supply, air cooler/dehumidifier, air humidifier, air heater, and surface heater) were engaged based on the weather scenario. An equilibration period was allowed to ensure the various atmospheric conditions achieve their desired values. Thereafter, the chamber lid was opened, the sample was mounted, a re-stabilization period allowed, the instrument was sealed, and the test data were recorded. During the experiment, the various gages were observed and re-adjusted to ensure the parameters remain consistent throughout.

Table 4 presents six evaporation estimation equations applicable to this study. For use in these equations, the experimental data in the BAS/BAS2 requires several analyzed parameters.

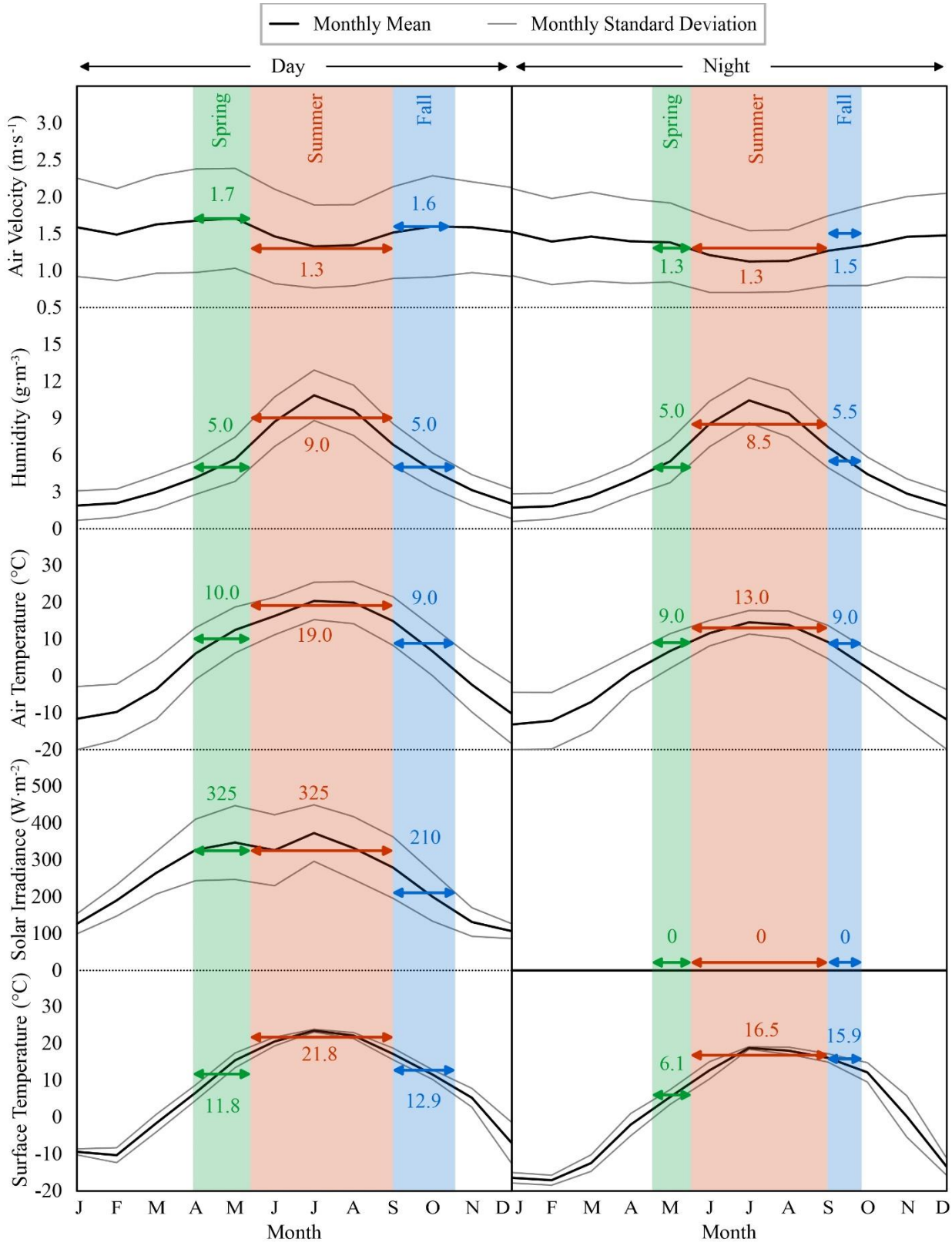

Figure 2. Summary of surface-atmosphere conditions in the semi-arid Canadian Prairies. Left column: daytime conditions, right column: nighttime conditions.

Table 3. Selected atmospheric parameters in the study area, after [12].

Weather Scenario	Date Range (Day)	Duration (Hours)	Air Velocity (m/s) [a]	Air Humidity (g/m^3) [b]	Air Temperature (°C)	Solar Irradiance (W/m^2) [c]	Surface Temperature (°C)
Day	84–334	3706					
Spring	94–149	883	1.7	5.0	10.0	325	11.8
Summer	150–254	1755	1.3	9.0	19.0	325	21.8
Fall	261–304	541	1.6	5.0	9.0	210	12.9
Night	110–317	1827					
Spring	122–148	206	1.3	5.0	9.0	0	6.1
Summer	149–253	761	1.3	8.5	13.0	0	16.5
Fall	254–279	277	1.5	5.5	9.0	0	15.9

[a] Downscaled from CWEEDS 10 m anemometer height to BAS 0.03 m height using the logarithmic law. [b] Absolute humidity (vapor density) calculated using CWEEDS dewpoint temperature and dry bulb temperature. [c] Global solar horizontal irradiance at the surface, shortwave spectrum (285 nm to 3 µm).

Table 4. Summary of empirical equations for estimation of evaporative flux, after [11].

Type and Reference	Evaporation Equation (g/m^2·s)
Mass-Transfer	
Himus and Hinchley (1924)	$1 \times 10^{-6}(64.58 + 28.06v)e_d$
Meyer (1942)	$1.06317 \times 10^{-7}\rho_w(1 + 0.1v)(e_d/1000)$
Penman (1948)	$3.3828 \times 10^{-8}\rho_w(1 + 0.24v)(e_d/1000)$
Combination	
Monteith (1965)	$\frac{1}{\lambda}\left(\frac{\Delta Q + 1.01\rho_a e_u / r_a}{\Delta + \gamma}\right)$
De Bruin and Keijman (1979)	$\frac{1}{\lambda}\left[\frac{\Delta Q}{(0.85\Delta) + (0.63\gamma)}\right]$
Duan and Bastiaanssen (2017)	$\frac{1}{\lambda}\left[\frac{Q - (1.01\rho_a[-0.17T_a + 4.27][1 + 0.536v])}{251}\right]$

The determination of these parameters is described herein. Air pressure is the force per unit area exerted by all gases in the climate chamber atmosphere and was measured (P_m; Pa) at 30-s intervals. Air pressure at 10 s intervals was interpolated (P_i; Pa) between the measurements at 0 s (P_{m0}) and 30 s (P_{m30}) using a linear relationship. Air density (ρ_a; g·m^{-3}), the mass per unit volume of all gases in the climate chamber atmosphere, was calculated at each atmospheric point was using interpolated air pressure (P_i; Pa), air temperature (T_a; °C), molar mass of dry air (M_a; 28.96546 g·mol^{-1}), molar mass of water (M_v; 1.801528 g·mol^{-1}), molar gas constant (R; 8.314472 J·mol^{-1}·°K^{-1}), mole fraction of water vapour (x_v) (Equation (2)), and compressibility factor (Z) (Equation (4)) with the equation [15]:

$$\rho_a = \frac{P \cdot M_a}{Z \cdot R \cdot (T_a + 273.15)} \cdot \left[1 - x_v\left(1 - \frac{M_v}{M_a}\right)\right] \quad (1)$$

The mole fraction of water (x_v) was calculated using interpolated air pressure (P_i; Pa), relative humidity (h; %), enhancement factor (f) (Equation (3)), and saturated vapor pressure (e_s; Pa) (Equation (7)) with the equation [15]:

$$x_v = h \cdot f \cdot \left(\frac{e_s}{P_i}\right) \quad (2)$$

The enhancement factor (f) was calculated using air temperature (T_a; °C), interpolated air pressure (P_i; Pa), and the constants A (1.00062), B (3.14 × 10^{-8} Pa^{-1}), and C (5.6 × 10^{-7} °C^{-2}) with the equation [15]:

$$f = A + B \cdot P + C \cdot T_a^2 \quad (3)$$

The compressibility factor (Z) was calculated using air temperature (T_a; °C), interpolated air pressure (P_i; Pa), mole fraction of water (x_v), and the constants a_0 –(1.58123 × 10^{-6} °K·Pa^{-1}), a_1 (−2.9331 × 10^{-8} Pa^{-1}), a_2 (1.1043 × 10^{-10} °K^{-1}·Pa^{-1}), b_0 (5.707 × 10^{-6} °K·Pa^{-1}), b_1 (−2.051 × 10^{-8} Pa^{-1}), c_0 (1.9898 × 10^{-4} °K·Pa^{-1}), c_1 (−2.376 × 10^{-6} Pa^{-1}), d_0 (1.83 × 10^{-11} °K^2·Pa^{-2}), and e_0 (−0.765 × 10^{-8} °K^2·Pa^{-2}), with the equation [15]:

$$Z = 1 - \frac{P_i}{T_a+273.15} \cdot [a_0 + a_1 \cdot T_a + a_2 \cdot T_a^2 + (b_0 + b_1 \cdot T_a) \cdot x_v + (c_0 + c_1 \cdot T_a) \cdot x_v^2] + \frac{P_i^2}{(T_a+273.15)^2} \cdot (d_0 + e_0 \cdot x_v^2) \quad (4)$$

Partial vapor pressure (e_a; Pa), the force per unit area exerted by gas-state water in the climate chamber atmosphere, was calculated at each atmospheric point using dew point temperature (T_d; °C) (Equation (6)) [16]:

$$e_a = 61.08 \cdot \exp\left(\frac{17.27 \cdot T_d}{T_d + 237.3}\right) \quad (5)$$

Dew point temperature (T_d; °C) was calculated using relative humidity (h; %) and air temperature (T_a; °C) with the equation [16]:

$$T_d = \frac{237.3\left(\frac{\ln(h/100)}{17.27} + \frac{T_a}{237.3+T_a}\right)}{1 - \left(\frac{\ln(h/100)}{17.27} + \frac{T_a}{237.3+T_a}\right)} \quad (6)$$

Saturated vapor pressure (e_s; Pa), the air temperature at which water vapor is in equilibrium with the upper surface boundary of liquid water, was calculated at each atmospheric point using air temperature (T_a; °C) or (T_s; °C) with the equation [17]:

$$e_s = 61.08 \cdot \exp\left(\frac{17.27 \cdot T_{a\ or\ s}}{237.3 + T_{a\ or\ s}}\right) \quad (7)$$

The vapor pressure deficit (e_d; Pa), the capacity in the atmosphere for water vapour to enter from the upper surface boundary of liquid water, was calculated at each atmospheric point using partial vapor pressure (e_a; Pa) (Equation (5)) and saturated vapor pressure (e_s; Pa) (Equation (7)) with the equation [18]:

$$e_d = e_s - e_a \quad (8)$$

Vapor density, the mass per unit volume of water vapor in the climate chamber atmosphere, was calculated at each atmospheric point using air temperature (T_a; °C) and partial vapor pressure (e_a; Pa) (Equation (5)) with the equation [16]:

$$\rho_v = \frac{2165 \cdot e_a}{1000 \cdot (T_a + 273.15)} \quad (9)$$

Vapor flux (Φ; g·m^{-2}·s^{-1}) represents a loss of mass by evaporation from the upper surface boundary. A positive value indicates a loss of mass with the vector away from the surface towards the atmosphere. Vapor flux was calculated using the sample mass rate of change (ΔM; g·s^{-1}) (Equation (11)) and area of the surface (A; m^2) (Equation (12)) with the equation:

$$\Phi = \frac{\Delta M}{A} \quad (10)$$

The sample mass was measured (M_m; g) in each scenario and fitted with a polynomial linear regression trendline. The curve-fit sample mass (M_c; g) was extracted using each trendline equation (Table 2). The sample mass rate of change (ΔM; g·s^{-1}) was calculated

using the change in curve-fit sample mass over 10 s time-step intervals (Δt; 10 s) with the equation:

$$\Delta M = \frac{M_c}{\Delta t} \tag{11}$$

The surface area (A; m^2), assumed to be perfectly horizontal throughout experimentation, was calculated at 10 s time-step intervals using a linear relationship with sample volume (V; $^{-3}$) (Equation (13)) in the sample container:

$$A = 15.547 \cdot V + 0.0013 \tag{12}$$

The sample volume (V; m^{-3}), equal to water volume, was calculated using the relationship with water mass (M_c; g), and density (ρ_w; $g \cdot m^{-3}$) (Equation (14)):

$$V = \frac{M_c}{\rho_w} \tag{13}$$

Water density (ρ_w; $g \cdot m^{-3}$) was calculated using the density of air-saturated water (ρ_s; $g \cdot m^{-3}$) (Equation (15)), thermal compressibility (κ_T; Pa^{-1}) (Equation (16)), and interpolated air pressure (P_i; Pa) with the equation [19]:

$$\rho_w = \rho_s \cdot [1 + \kappa_T \cdot (P_i - 101325)] \tag{14}$$

The density of air-saturated water (ρ_s; $g \cdot m^{-3}$) was calculated using surface temperature (T_s; °C) with the equation [19]:

$$\rho_s = 999.84847 + 6.337563e^{-2} \cdot T_s - 8.523829e^{-3} \cdot T_s^2 + 6.943248e^{-5} \cdot T_s^3 - 3.821216e^{-7} \cdot T_s^4 \tag{15}$$

Isothermal compressibility (κ_T; Pa^{-1}) was calculated using surface temperature (T_s; °C) with the equation [19]:

$$\kappa_T = 50.83101e^{-8} - 3.68293e^{-9} \cdot T_s + 7.263725e^{-11} \cdot T_s^2 - 6.597702e^{-13} \cdot T_s^3 + 2.87767e^{-15} \cdot T_s^4 \tag{16}$$

Applying conservation of energy at the surface, the energy balance calculated using heat storage (Q; $W \cdot m^{-2}$), net radiant heat flux (R_n; $W \cdot m^{-2}$), ground heat flux (G_0; $W \cdot m^{-2}$), sensible heat flux (H; $W \cdot m^{-2}$), and evaporative heat flux (λE; $W \cdot m^{-2}$) with the equation:

$$Q = R_n - G_0 - H - \lambda E \tag{17}$$

Assuming an infinitely thin surface, the heat storage is set to equal zero. The difference between net radiant heat flux and ground heat flux ($R_n - G_0$) is defined as the available energy (AE) in the rearranged equation [20]:

$$AE = R_n - G_0 = H + \lambda E \tag{18}$$

Net radiant heat flux (R_n; $W \cdot m^{-2}$) represents a gain or loss of energy by radiant heat transfer from the upper surface boundary. A positive value indicates a gain of energy with the vector away from the atmosphere towards the surface. Net radiant heat flux was calculated using incoming shortwave (S_i; $W \cdot m^{-2}$), incoming longwave (L_i; $W \cdot m^{-2}$), outgoing shortwave (S_o; $W \cdot m^{-2}$), and outgoing longwave (L_i; $W \cdot m^{-2}$) radiant energy with the equation:

$$R_n = (S_i + L_i) - (S_o + L_o) \tag{19}$$

Incoming longwave irradiation (L_i; $W \cdot m^{-2}$) was calculated and averaged between the low-upwind and low-downwind atmospheric points using air temperature (T_a; °C),

air emissivity (ε_a) (Equation (19)), and the Stefan–Boltzmann constant (σ; 5.670·× 10^{-8} W·m^{-2}·°C^{-4}) with the equation [21]:

$$L_i = \varepsilon_a \cdot \sigma \cdot (T_a + 273.15)^4 \quad (20)$$

Air emissivity (ε_a) was calculated using air temperature (T_a; °C) and partial vapor pressure (e_a; Pa) (Equation (5)) with the equation [22]:

$$\varepsilon_a = 0.7 + 5.95e^{-5} \cdot \left(\frac{e_a}{100}\right) \cdot \exp\left(\frac{1500}{273.15 + T_a}\right) \quad (21)$$

Outgoing shortwave radiation (S_o; W·m^{-2}) was measured by an albedometer positioned as close to the zenith of the sample as the chamber design allowed. As the surface of the sensor was placed closer to the sample surface than the lightbulb, Newton's inverse square law was used to correct for the height difference, using S_m as the measured reflected shortwave irradiance (W·m^{-2}), D_m as the height of the albedometer sensor above the sample surface (mm), and D_l as the height of the light bulb above the sample surface (mm) with the equation:

$$S_o = \frac{S_m \cdot D_m^2}{D_l} \quad (22)$$

Outgoing longwave radiation (L_o; W·m^{-2}) was calculated using surface temperature (T_s; °C), surface emissivity (ε_s; 0.980 [23]), and the Stefan–Boltzmann constant (σ; 5.670 × 10^{-8} W·m^{-2}·°K^{-4}) with the equation [21]:

$$L_o = \varepsilon_s \cdot \sigma \cdot (T_s + 273.15)^4 \quad (23)$$

Evaporative heat flux (λE; W·m^{-2}) represents a loss of energy by latent heat transfer from the upper surface boundary. A positive value indicates a loss of energy with the vector away from the surface towards the atmosphere and was calculated using the rate of evaporative latent heat ($\Delta\lambda E$; W) (Equation (25)) and the area of the surface (A; m^2) (Equation (12)) with the equation:

$$\lambda E = \frac{\Delta\lambda E}{A} \quad (24)$$

The rate of evaporative latent heat ($\Delta\lambda E$; W) was calculated using the latent heat of water vaporization (λ; J·g^{-1}) (Equation (26)) and the sample mass rate of change (ΔM; g·s^{-1}) (Equation (11)) with the equation:

$$\Delta\lambda E = \Delta M \cdot \lambda \quad (25)$$

The latent heat of water vaporization (λ; J·g^{-1}) was calculated using surface temperature (T_s; °C) with the equation [17]:

$$\lambda = 1000 \cdot \left(2.501 - 2.361e^{-3} \cdot T_s\right) \quad (26)$$

Sensible heat flux (H; W·m^{-2}) represents the loss or gain of energy by convective and conductive heat transfer through the upper surface boundary. A positive value indicates a loss of energy with the vector away from the surface towards the atmosphere and was calculated using the Bowen ratio (β) relationship with latent heat flux (λE; W·m^{-2}) (Equation (24)):

$$H = \beta \cdot \lambda E \quad (27)$$

The Bowen ratio was calculated by applying the aerodynamic method [24] and validated by confirming $\beta \neq -0.75$ to -1.25 [25]. Low-downwind air temperature (T_{ald}; °C) and vapour density (ρ_{vld}; g·m^{-3}) (Equation (5)) and high-downwind air temperature (T_{ahd}; °C) and vapor density (ρ_{vhd}; g·m^{-3}) (Equation (5)) atmospheric points were used, as well

as air density (ρ_a; g·m^{-3}) (Equation (1)) averaged between the two atmospheric points, isobaric specific heat of air (C_p; 1.010 J·g^{-1}·°C^{-1}), and latent heat of water vaporization (λ; J·g^{-1}) (Equation (26)) using the equation [20]:

$$\beta = \frac{\rho_a \cdot C_p \cdot (T_{ald} - T_{ahd})}{\lambda \cdot (\rho_{vld} - \rho_{vhd})} \tag{28}$$

Ground heat flux (G_0; W·m^{-2}) represents the loss or gain of energy by conductive heat transfer through the lower surface boundary. A positive value indicates a loss of energy with the vector away from the surface towards the ground, and was calculated using radiant heat flux (R_n; W·m^{-2}) (Equation (19)), sensible heat flux (H; W·m^{-2}) (Equation (27)), and evaporative heat flux (λE; W·m^{-2}) (Equation (24)), with the equation [20]:

$$G_0 = R_n - H - \lambda E \tag{29}$$

Aerodynamic resistance (r_a; s·m^{-1}) affects the movement of vapor into the atmosphere by turbulent diffusion and was calculated using measured air velocity (v; m·s^{-1}), and heights of the low up-wind thermometer–hygrometer sensors (m) [17]:

$$r_a = \frac{4.72 \cdot \left[\ln\left(\frac{0.03}{0.0005}\right)\right]^2}{1 + 0.536} \tag{30}$$

The psychrometric constant (γ; Pa·°C^{-1}) is a relationship between partial vapor pressure and air temperature and was calculated using interpolated air pressure (e_a; Pa) and latent heat of water vaporization (λ; J·g^{-1}) (Equation (26)) [17]:

$$\gamma = \frac{e_a \cdot 1.1013}{\lambda \cdot 0.622} \tag{31}$$

The vapor pressure gradient (Δ; Pa·°C^{-1}) is the gradient of the saturated vapor pressure function and was calculated using saturated vapor pressure (e_s; Pa) (Equation (7)) and measured air temperature (T_a; °C) [17]:

$$\Delta = \frac{e_s \cdot 4098}{(234.3 + T_a)^2} \tag{32}$$

The rate of evaporation (E; mm/day) is a common representation of evaporative water loss and was calculated using vapor flux (Φ; g·m^{-2}·s^{-1}) (Equation (10)) and water density (ρ_w; g·m^{-3}) (Equation (14)):

$$E = 86,400\left(\frac{\Phi \cdot 1000}{\rho_w}\right) \tag{33}$$

Author Contributions: Data curation and analysis, J.S.; supervision, S.A.; writing—original draft, J.S.; writing—review and editing, S.A. All authors have read and agreed to the published version of the manuscript.

Funding: Natural Science and Engineering Research Council of Canada.

Institutional Review Board Statement: Not applicable.

Informed Consent Statement: Not applicable.

Data Availability Statement: The root data folder was last accessed on 12 November 2021. The folder can be downloaded from https://dataverse.scholarsportal.info/dataverse/liquid-evaporation.

Acknowledgments: The authors would like to thank the University of Regina for providing laboratory and data repository space.

Conflicts of Interest: The authors declare there is no conflicts of interest.

Abbreviations

Item	Symbol	Unit
Aerodynamic Resistance	r_A	s/m
Air Emissivity	ε_A	Dimensionless
Air Pressure (Interpolated)	e_A	Pa
Air Pressure (Measured)	e_{AM}	Pa
Air Velocity	v	m/s
Available Energy	Q	W/m^2
Bowen Ratio	β	Dimensionless
Compressibility Factor	Z	Dimensionless
Density (Air)	ρ_A	g/m^3
Density (Vapour)	ρ_V	g/m^3
Density (Water, Air Saturated)	ρ_{WS}	g/m^3
Density (Water, Corrected)	ρ_W	g/m^3
Enhancement Factor	f	Dimensionless
Evaporation Rate	E	mm/day
Evaporative Latent Heat	λ	J/g
Evaporative Latent Heat Flow	$\Delta\lambda E$	W
Heat Flux (Conductive Thermal)	G	W/m^2
Heat Flux (Evaporative Latent)	λE	W/m^2
Heat Flux (Longwave Radiant, Incoming)	L_i	W/m^2
Heat Flux (Longwave Radiant, Outgoing)	L_O	W/m^2
Heat Flux (Net Radiant)	R_n	W/m^2
Heat Flux (Sensible Thermal)	H	W/m^2
Heat Flux (Shortwave Radiant, Incoming)	S_i	W/m^2
Heat Flux (Shortwave Radiant, Outgoing Corrected)	S_O	W/m^2
Heat Flux (Shortwave Radiant, Outgoing Measured)	S_{OM}	W/m^2
Isothermal Compressibility	κ_T	Dimensionless
Mole Fraction of Water Vapour	X	Dimensionless
Psychrometric Constant	γ	Pa/°C
Relative Humidity	h	%
Sample Mass (Interpolated)	M	g
Sample Mass (Measured)	M_M	g
Sample Mass (Rate of Change)	ΔM	g/s
Sample Surface Area	A	m^2
Sample Volume	V	m^3
Temperature (Air)	T_A	°C
Temperature (Dew Point)	T_D	°C
Temperature (Surface)	T_S	°C
Vapour Flux	Φ	$g/s{\cdot}m^2$
Vapour Pressure (Deficit)	e_D	Pa
Vapour Pressure (Gradient)	Δ	Pa/°C
Vapour Pressure (Partial)	e_V	Pa
Vapour Pressure (Saturated, Atmosphere)	e_S	Pa
Vapour Pressure (Saturated, Surface)	e_f	Pa

References

1. Roberts, K.; Cahill, C.; Soulard, F.; Wang, J.; Henry, M.; Gagnon, G. *Human Activity and the Environment: Freshwater in Canada*; Catalogue No. 16-201-X; Statistics Canada: Ottawa, ON, Canada, 2017.
2. Lemmen, D.S.; Vance, R.E.; Campbell, I.A.; David, P.P.; Pennock, D.J.; Sauchyn, D.J.; Wolfe, S.A. *Geomorphic Systems of the Palliser Triangle, Southern Canadian Prairies: Description and Response to Changing Climate*; Natural Resources Canada: Ottawa, ON, Canada, 1998.
3. Teller, J.T.; Moran, S.R.; Clayton, L. The Wisconsinan deglaciation of southern Saskatchewan and adjacent areas: Discussion. *Can. J. Earth Sci.* **1980**, *17*, 539–541. [CrossRef]
4. Trenberth, K.E. Changes in precipitation with climate change. *Clim. Res.* **2011**, *47*, 123–138. [CrossRef]
5. Pomeroy, J.W.; Shook, K.R. *Review of Lake Diefenbaker Operations 2010–2011*; Centre for Hydrology, University of Saskatchewan: Saskatoon, SK, Canada, 2012.

6. Ito, M.; Azam, S. Feasibility of Saline Gradient Solar Ponds as Thermal Energy Sources in Saskatchewan, Canada. *J. Environ. Inform. Lett.* **2019**, *1*, 72–80. [CrossRef]
7. Hammer, U.T. Saline Lake Resources of the Canadian Prairies. *Can. Water Resour. J.* **1986**, *11*, 43–57. [CrossRef]
8. Finch, J.W.; Calver, A. *Methods for the Quantification of Evaporation from Lakes*; Centre for Ecology & Hydrology: Wallingford, UK, 2008.
9. Trautz, A.C.; Illangasekare, T.H.; Howington, S. Experimental testing scale considerations for the investigation of bare-soil evaporation dynamics in the presence of sustained above-ground airflow. *Water Resour. Res.* **2018**, *54*, 8963–8982. [CrossRef]
10. Suchan, J.; Azam, S. Development of BAS2 for determination of evaporative fluxes. *MethodsX* **2021**, *8*, 101424. [CrossRef] [PubMed]
11. Suchan, J.; Azam, S. Determination of Evaporative Fluxes Using a Bench-Scale Atmosphere Simulator. *Water* **2021**, *13*, 84. [CrossRef]
12. Suchan, J.; Azam, S. Effect of Salinity on Evaporation from Water Surface in Bench-Scale Testing. *Water* **2021**, *13*, 2067. [CrossRef]
13. Suchan, J.; Azam, S. Liquid Evaporation Database. *Sch. Portal Dataverse* **2021**, *1*. [CrossRef]
14. Hulley, G. *MYD21A2 MODIS/Aqua Land Surface Temperature/3-Band Emissivity 8-Day L3 Global 1km SIN Grid V006*; NASA EOSDIS Land Processes DAAC: Oak Ridge, TN, USA, 2017.
15. Picard, A.; Davis, R.S.; Gläser, M.; Fujii, K. Revised formula for the density of moist air (CIPM-2007). *Metrologia* **2008**, *45*, 149–155. [CrossRef]
16. Snyder, R.L. *Humidity Conversion*; UC Davis Biometeorology Group: Davis, CA, USA, 2005.
17. Shuttleworth, W.J. Evaporation. In *Handbook of Hydrology*; Maidment, D.R., Ed.; McGraw-Hill Inc.: New York, NY, USA, 1993; pp. 4.1–4.53.
18. Yuan, W.; Zheng, Y.; Piao, S.; Ciais, P.; Lombardozzi, D.; Wang, Y.; Ryu, Y.; Chen, G.; Dong, W.; Hu, Z.; et al. Increased atmospheric vapor pressure deficit reduces global vegetation growth. *Sci. Adv.* **2019**, *5*, 1–12. [CrossRef] [PubMed]
19. Jones, F.E.; Harris, G.L. ITS-90 density of water formulation for volumetric standards calibration. *J. Res. Natl. Inst. Stand. Technol.* **1992**, *97*, 335–340. [CrossRef] [PubMed]
20. Granger, R.J.; Gray, D.M. Evaporation from natural nonsaturated surfaces. *J. Hydrol.* **1989**, *111*, 21–29. [CrossRef]
21. An, N.; Hemmati, S.; Cui, Y. Assessment of the methods for determining net radiation at different time-scales of meteorological variables. *J. Rock Mech. Geotech. Eng.* **2017**, *9*, 239–246. [CrossRef]
22. Idso, S.B. A set of equations for full spectrum and 8- to 14-μm and 10.5- to 12.5-μm thermal radiation from cloudless skies. *Water Resour. Res.* **1981**, *17*, 295–304. [CrossRef]
23. Robinson, P.; Davies, J. Laboratory determinations of water surface emissivity. *J. Appl. Meteorol.* **1972**, *11*, 1391–1393. [CrossRef]
24. Malek, E. Comparison of the Bowen ratio-energy balance and stability-corrected aerodynamic methods for measurement of evapotranspiration. *Theor. Appl. Climatol.* **1993**, *48*, 167–178. [CrossRef]
25. Payero, J.O.; Neale, C.M.U.; Wright, J.L.; Allen, R.G. Guidelines for validating Bowen Ratio data. *Trans. Am. Soc. Agric. Eng.* **2003**, *46*, 1051–1060. [CrossRef]